Title

"Virtual Shear Box" experiments of stress and slip cycling within a subduction interface mélange

Short Title

Subduction mélange stress and slip cycling

Authors

Sam Webber[1,2*], Susan Ellis[2], Åke Fagereng[3]

Affiliations

[1] Victoria University of Wellington, Wellington.

[2] GNS Science, Lower Hutt.

[3] Cardiff University, Cardiff.

*Correspondence to: samuel.m.webber@gmail.com

Keywords: subduction; mélange; stress; numerical modeling; Chrystalls Beach Complex; strain transients

1 ABSTRACT

What role does the progressive geometric evolution of subduction-related mélange shear zones play in the development of strain transients? We use a “virtual shear box” experiment, based on outcrop-scale observations from an ancient exhumed subduction interface - the Chrystalls Beach Complex (CBC), New Zealand - to constrain numerical models of slip processes within a meters-thick shear zone. The CBC is dominated by large, competent clasts surrounded by interconnected weak matrix. Under constant slip boundary conditions, models of the CBC produce stress cycling behavior, accompanied by mixed brittle-viscous deformation. This occurs as a consequence of the reorganization of competent clasts, and the progressive development and breakdown of stress bridges as clasts mutually obstruct one another. Under constant shear stress boundary conditions, the models show periods of relative inactivity punctuated by aseismic episodic slip at rapid rates (meters per year). Such a process may contribute to the development of strain transients such as slow slip.

2 INTRODUCTION

Subduction megathrust faults can exhibit a wide range of slip behaviors (e.g., Ide et al., 2007; e.g., Peng and Gomberg, 2010). Some are interseismically locked to ~20-30 km depths, accumulating stress slowly between large earthquakes, and transitioning to steady aseismic creep at greater depths where temperatures exceed those required for quartz plasticity (>350°C; e.g., Hyndman and Wang, 1993). Other megathrust faults can experience punctuated slow slip events (SSEs) – characterized by aseismic creep that occurs at rates that are subseismic but faster than plate boundary averages – that last for days to years (e.g., Miyazaki et al., 2006; Peng and Gomberg, 2010). Slow slip rates are commonly 0.15 – 1.0 m year^{-1}, and up to ~2 cm day^{-1} (e.g., Miyazaki et al., 2006; Schwartz and Rokosky, 2007; Wallace and Beavan, 2010; Bartlow et al., 2014). Transient slow slip is commonly associated with episodic tectonic tremor and/or microseismicity, and may play a significant role in stress cycling at subduction zones (Ide et al., 2007; Schwartz and Rokosky, 2007; Peng and Gomberg, 2010). Many SSEs occur at depths of >20–30 km, although they have also been detected at <5–20 km depths (e.g., Wallace et al., 2012; Araki et al., 2017). Several recent explanations for shallow episodic tremor and slip (ETS) focus on the transitional frictional behavior of clays, and the effects of evolving clay mineralogy on frictional stability and strength with increasing pressure and temperature, based on experimental deformation of clay- and quartz-rich gouges (e.g., Ikari and Saffer, 2011; den Hartog et al., 2012; Ikari et al., 2013; Ikari et al., 2015). Other explanations relate to frictional stability variations resulting from low normal stresses associated with zones of highly overpressured fluids, and the effects of heterogeneous stresses and materials (e.g., Scholz, 1998, 2002; Liu and Rice, 2005, 2007; Skarbek et al., 2012; Wang and Bilek, 2014; Saffer and Wallace, 2015, and references therein).

Laboratory experiments on clay- and quartz-rich gouges have documented the effects of evolving clay mineralogy on frictional stability and strength with pressure and temperature (e.g., Ikari et al., 2013; Saito et al., 2013). Such shear box experiments typically deform mm-thick gouge layers. In contrast, studies of exhumed subduction faults suggest that at $\gtrsim$1 km depths, the subduction interface between upper and lower plates at convergent margins can be hundreds of meters wide, with multiple discrete, anastomosing, simultaneously active fault strands organized within 5-35 m thick tabular high-strain zones (Rowe et al., 2013). Exhumed subduction thrusts also exhibit a complex rheological mix of materials that have experienced mixed brittle fracturing, ductile shear, and solution-precipitation creep, accompanied by transient near-lithostatic fluid pressure cycling (e.g., Bachmann et al., 2009; Fagereng and Sibson, 2010; Fagereng, 2011a; Hayman and Lavier, 2014). To date, only a few attempts have been made to capture such complex rheological interactions using laboratory and numerical experiments (e.g., Skarbek et al., 2012; Reber et al., 2015).

Here, we attempt to understand subduction zone slip behavior at scales greater than those attained in laboratory experiments, by simulating a “virtual shear box” using numerical modeling. We deform a two-phase mélange, volumetrically dominated by large competent clasts, surrounded by a weak interconnected matrix. Our results suggest that geometric reorganization within a subduction mélange can drive significant oscillations in shear stress and/or slip velocities of durations and frequencies of months to years.

3 CHRYSTALLS BEACH COMPLEX: AN ANCIENT SUBDUCTION ANALOGUE

The initial distribution and rock materials in our model domain are based on field exposures of the Chrystalls Beach Complex (CBC), New Zealand. The CBC is a <4 km thick tectonic mélange deformed along an ancient subduction interface between 175–155 Ma, at <550 MPa and ~300°C peak metamorphic conditions (Fagereng and Cooper, 2010; Fagereng, 2011a, and references therein). Within the CBC, asymmetric competent clasts of sandstone, chert and basalt – themselves derived from non-coaxial shear and layer-perpendicular shortening of original bedding – are surrounded by a weak phyllitic matrix (Fagereng, 2011a). The frequency-size distributions of competent lenses follow a power-law distribution, where the power law exponent depends on the volume ratio of competent to incompetent material (Fagereng, 2011b). The competent clasts contain internal fault-fracture networks comprising extension fractures that are dominantly oriented perpendicular to clast long axes (Fagereng, 2011b).

The CBC has been intensely sheared in a mixed continuous-discontinuous style, where discontinuous deformation records localized seismic and/or aseismic slip adjacent to volumetrically continuous fabrics that have experienced aseismic flow (Fagereng and Sibson, 2010, and references therein). Exposures express a complex superposition of deformation structures, indicating formation in a time-progressive sequence of increasing cohesive strength (Fagereng, 2011a). Fagereng (2011a) has suggested that within the CBC, different mineral-scale deformation mechanisms, the degree of continuous versus discontinuous deformation, and bulk rheological behavior, all depend on the local volumetric ratio of competent clasts to matrix, and that transient, locally high fluid pressures were required to form slickenfibres, extension fractures, and vein deposits.

4 THE “VIRTUAL SHEAR BOX”

The finite element code SULEC (Buiter and Ellis, 2012) is used to model aseismic slip in a “virtual shear box” that represents a portion of an actively deforming subduction thrust interface, which may itself be up to hundreds of meters thick (Rowe et al., 2013). We use a representative clast-dominated mélange configuration from the CBC (Fagereng and Sibson, 2010), characterized by ~70% competent clasts and ~30%

mudstone matrix (Fig. 1). The exposure is representative of a clast-dominated zone within the mélange; this differs from zones where the matrix is volumetrically dominant, and bulk steady creep inferred to have occurred (Fagereng and Sibson, 2010). We assume that the current observed outcrop configuration approximates the subduction system immediately prior to exhumation, such that it is appropriate for modeling deformation at peak metamorphic conditions. Therefore, we do not model a time-progressive increase in clast cohesion – rather we hold the model domain at a constant depth for the duration of the model run (which lasts for months – decades).

We apply a composite matrix rheology, including a combination of pressure-sensitive Coulomb yield and linear precipitation-solution creep, derived from a microphysical model of phyllosilicate gouge (Niemeijer and Spiers, 2005; Den Hartog and Spiers, 2013; Fagereng and den Hartog, 2017), and viscous non-linear dislocation creep (Supplement S1), (Mares and Kronenberg, 1993; Bukovská et al., 2016). At each time-step, the deformation mechanism (frictional shear combined with pressure solution, or non-linear creep) is determined at each node as the mode of lowest yield stress. The strong cohesive clasts may only deform brittlely, and have a Byerlee friction coefficient of 0.72, and cohesive strength of 70 MPa (see Supplement S1). Our experiments are run at 250°C, lithostatic pressure corresponding to 20 km depth (520 MPa, assuming a bulk rock density of 2650 kg m^{-3}), and constant fluid pressure ratios $\lambda = (P_f/\sigma_z)$ of 0.67, 0.8 or 0.9, where P_f is fluid pressure, and σ_z is overburden stress. Here we assume that fluid pressure is greater than hydrostatic (i.e., λ=0.38), and may approach lithostatic values ($\lambda \geq 0.9$) consistent with structural interpretations of Fagereng et al. (2010) from orientations and microstructures of shear and extension veins within the CBC. In order to simplify modeling, we do not allow tensile hydrofractures to occur; instead, we impose a lower cutoff to maintain effective stresses at a small positive value (effectively reducing rock yield strength to a lower limit of 1 MPa). Implicit in this simplification is an assumption of volume conservation within the model domain. Given that tensile veins in mélanges are commonly filled by locally derived materials (e.g., Fisher et al., 1995), and that the microphysical model for frictional-viscous creep assumes microscale material transport around quartz clasts (den Hartog and Spiers, 2014), we acknowledge the possibility of long-term volume changes within mélanges, but expect that a closed system behavior at the scale of our model is reasonable approximation at the modeled time scales.

5 EXPERIMENT 1: CONSTANT VELOCITY EXPERIMENTS

In experiment 1, a uniform horizontal velocity is applied at the upper boundary (V_{top}), above a fixed lower boundary. We measure the average shear stress at the upper boundary (τ_{top}) required to deform the mélange at a prescribed V_{top} – either 5 cm year^{-1} (i.e., plate tectonic rates; Fig. *2*a), or 3 cm week^{-1} (i.e., rates representative of slow slip on the northern Hikurangi Margin; Fig. *2*b), (Wallace and Beavan, 2010). This experiment is analogous to an experimental shear box apparatus that deforms at constant velocity, only at larger scale.

Fig. 2a and b illustrate that the τ_{top} necessary to deform the modeled mélange depends on the fluid pressure ratio λ, with lower stresses required for higher λ. These models experience significant temporal variations in τ_{top} for a given λ, with variations of up to 70% of the time-averaged shear stress. For example, for V_{top} = 5 cm year^{-1}, the τ_{top} required to deform the model domain can vary between 35 – 60 MPa (λ = 0.67), 20 – 48 MPa (λ = 0.8), and 2 – 30 MPa (λ = 0.9; Fig. 2a). These stress fluctuations result from the reorganization of clast geometry over time, as clasts interact and transmit stress. Stress cyclicity is a function of the clast-dominated model architecture, where mutually obstructing competent clasts force strain to localize into narrow adjacent matrix channels (Fig. 3). Tightly-packed clasts form stress bridges that dip in the direction of slip (cf., Deubelbeiss et al., 2011; Hayman and Lavier, 2014) - where we define stress bridges as parts of the model domain where shear stresses exceed 100 MPa. When clasts obstruct matrix pathways, actively straining matrix channels are more distributed and less interconnected throughout the model area, and experience lower strain-rates. Stress bridges develop between adjacent clasts (orange shaded areas, Fig. 3a, Fig. 3c). When clasts are instead widely spaced and matrix pathways are unobstructed, strain localizes onto a small number of interconnected matrix pathways, and little force is transmitted between the clasts (i.e., devolved stress bridges; Fig. 3b). This interplay results in an oscillation between a state where the model is characterized by an interconnected weak matrix, and one where elevated shear stresses are supported by a strong load-bearing framework. Stress cycling continues indefinitely for larger amounts of shear strain (γ) than is shown in Fig. 2 ($\gamma \gtrsim$ 6.0), because block rotation (which inhibits and/or disrupts the development of through-going layers of matrix material) competes with progressive clast disaggregation.

Shear stress fluctuations can be converted to effective friction coefficients. A bulk Coulomb friction coefficient for the entire model is calculated by dividing τ_{top} by the effective overburden stress. The higher the pore fluid pressure ratio, the lower the effective friction coefficient – this can be very low, e.g., for λ = 0.8 it is ~0.06. This effective friction coefficient has the same temporal cycling as seen in the stress plots in Fig. 2a.

Shear strain preferentially localizes within the phyllitic matrix and along the edges of competent clasts. Where matrix shear pathways are forced to localize onto narrow channels between interacting clasts, the matrix deforms partly by frictional sliding/pressure solution, and partly by nonlinear phyllosilicate dislocation creep where shear pathways widen and strain-rates are reduced. The active matrix deformation mechanism is controlled by the effective stress, shear strain rate ($\dot{\gamma}$), and temperature at each node. Despite the fluid pressure ratio λ being held constant in each model run, interactions between competent clasts and stress bridges between them can cause large variations in dynamic stresses, sometimes causing effective pressure to locally drop to zero where clast interactions lead to extensional stresses (Fig. 3, right-hand panels). Interestingly, this effect is greatest for the model where the fluid pressure ratio are modest (e.g., λ = 0.67, 0.8) rather than at higher fluid pressures (e.g., λ = 0.9); this is because dynamic stresses are reduced for the high fluid pressure experiment. Fig. 3 also illustrates that the principal compressive stress direction at each node can vary by up to ±45° from the expected orientation of ~45°. Local stress rotations occur as clast geometry and matrix pathways evolve, causing locally elevated dynamic stress effects.

Fig. 2 demonstrates short-period stress fluctuations of a few MPa, superimposed on longer time-scale cyclic stress oscillations. Short-term fluctuations result from individual clast interactions, while the longer timescale oscillation reflects wholescale development and break-down of stress bridges across the model. Longer timescale stress oscillations have a period that depends on V_{top} (Fig. 2a versus b), since the rate of geometric reorganization depends on the speed at which the box is shearing. For example, when the box is sheared at 5 cm year^{-1}, spectral analysis of Fig. 2a indicates that large-scale stress changes occur over a superposition of periods of ~years to tens of years, whereas when V_{top} = 3 cm week^{-1} they occur over periods of months to years (Fig. 2b). The periodicity in these models is not very regular, owing to the complex geometry derived from outcrop scale. The periodicity derived from such an outcrop-scale volume would be expected to average out for deformation over a shear zones at larger scales of ~100 m – 1 km. The periodicity of stress cyclicity also depends on the thickness of the deforming region, for a constant V_{top}. If deformation is distributed over multiple anastomosing shear zones at a larger scale than we have modelled, then a given V_{top} will result in lower strain-rates, increasing the period of stress cyclicity. For example, if our model domain accommodated 20% of the total subduction zone slip rate, then for tectonic rates of 5 cm year^{-1} stress cyclicity would have a period of 25 – 300 years.

6 EXPERIMENT 2: CONSTANT SHEAR STRESS EXPERIMENTS

In experiment 2 (Fig. 4a, b) we hold the fluid pressure ratio constant at λ = 0.8, and apply a constant shear stress at the upper boundary (τ_{top}), while we allow the slip velocity at the upper boundary V_{top} to vary freely. The shear stress imposed on the modeled subduction mélange section is constant in time. Sufficiently high τ_{top} results in time-variable cycling in V_{top}, while lower applied shear stress is insufficient to deform the box. To illustrate this, we apply a constant τ_{top} of 32 MPa (equal to the average shear stresses required to deform the model domain in experiment 1 for λ = 0.8), (Fig. 4; cf. Fig. 2a, b). As stress bridges disintegrate and redevelop within the model domain (inset panels, Fig. 4a), the resistance of the modeled mélange to the imposed shear stress fluctuates – this causes periods of low slip speed interspersed by period of high slip speed (up to m year^{-1}). The model exhibits a rough periodicity in time at about 2 – 5 years, although it is not very regular (Fig. 4a). The corresponding plot of slip velocity versus total slip at the top of the box (Fig. 4b) is more regular, because periods with low slip velocity do not contribute to total slip.

The higher the applied τ_{top}, the higher the average V_{top} (Fig. 5, Fig. *6*). For τ_{top} = 34 MPa, slip speeds are up to 20 m year^{-1}, and slip speeds above a minimum threshold of 5 cm year^{-1} occur more frequently than for lower applied shear stresses (Fig. 5). The model continues to creep at low strain-rates between major slip events. If the applied τ_{top} is insufficient to induce any response in the shear box (such that $V_{top} \rightarrow 0$), the model domain becomes permanently locked. In a real subduction setting, this state would persist until τ_{top} increases due to the steady accumulation of elastic strain and plate tectonic loading, or due to a perturbation in regional stresses and/or fluid pressure state occurs – for example due to a nearby earthquake, slip of adjacent parts of the interface, or fluid generation/release on or below the subduction interface.

7 DISCUSSION

The experiments run at constant V_{top} (experiment 1), and at constant τ_{top} (experiment 2), show cyclical stress and slip behavior on timescales of weeks to years. The constant stress numerical models predict aseismic slip transients at rates of up to meters year^{-1}, despite the model not incorporating the transition to velocity-weakening behavior at very high strain-rates (Fig. 4, Fig. 5). Cyclical stress and slip behaviors in experiments 1 and 2 are clearly linked to the progressive development of transient stress bridges that arise from interaction between competent clasts in a mélange matrix, where slip is accommodated by mixed brittle-viscous deformation (Fig. 3, Fig. 4). In models run at constant shear stress (experiment 2), transient slip events are marked by rapid reorganization of competent clasts along localized shear zones and consequent degradation of stress bridges, and are accompanied by elevated frictional-viscous creep rates in surrounding matrix shear pathways (e.g., Fig. 4a, top inset). Competent clasts within a clast-dominated mélange fail brittlely when subjected to elevated shear stresses, because of obstruction by other competent clasts. Transient slip events rapidly terminate as clasts impact one another, re-establishing stress bridges (e.g., Fig. 4a, bottom inset).

Our model experiments are subject to several assumptions and limitations. Significantly, we have restricted slip transients to speeds below dynamic rupture propagation. Whereas the frictional rheology we use is partly strain-rate dependent (Supplement S1), we have imposed a maximum slip rate to limit velocity weakening as stress bridges unload and matrix pathways become open. This allows us to explore slip transients similar in magnitude to those found during slow slip events for the accumulation of large finite strains in the virtual shear box, although this also means that our model runs are not representative of the entire seismic cycle.

It should also be noted that because these experiments were run in two dimensions, the magnitudes of stress fluctuations may be overestimated, due to greater matrix connectivity in three dimensions, and the ability of mutually obstructed clasts to move in the third dimension (e.g., Mair and Hazzard, 2007). In experiment 1, the timing and magnitude of stress cycling is controlled by the imposed V_{top} and λ, each assumed to be constant. Furthermore, in all model runs, stress cycling characteristics also depend on the exact initial model geometry (e.g., Fagereng and Sibson, 2010; Cyprych et al., 2016), the volumetric ratio of clast to matrix material (e.g., Ji et al., 2003), and relative material strengths.

7.1 SCALING OUTCROP MODELS OF STRESS AND SLIP CYCLING UP TO SUBDUCTION FAULTS

To understand the wider implications of our model experiments, they must be considered in the context of a larger plate-boundary subduction interface. Our results support the idea that a real subduction mélange (in which both V_{top} and τ_{top} are free to vary) may experience transient deformation driven by geometric reorganization of clasts within a weaker matrix. Experiments 1 and 2 show that – even in the absence of other transient mechanisms, such as variable fluid pressure, and a conditionally stable rheology – a deforming subduction mélange may experience significant natural variability in both slip rate and shear stress during the interseismic period.

During subduction deformation, any part of the mélange shear zone is connected laterally and vertically with a larger deforming system that may contain several anastomosing shear zones at scales of ~1 – 100 meters (Rowe et al., 2013). Any outcrop-scale stress or slip fluctuations (such as those modeled here) are likely to be out of phase with those within adjacent volumes, canceling each other out. However, the power-law distribution of clast geometries within the CBC (Fagereng, 2011b) can be used to infer behavior at larger scales. Mélange volumes with high clast density (such as that modeled here) form aggregate volumes at larger scales, surrounded by large matrix-dominated volumes (Fagereng, 2011a). These 10 – 100 m scale aggregates will interact to produce stress and strain transients in much the same way as our outcrop-scale mélange domain. If these aggregate volumes are of approximately the same scale as the width of the subduction thrust interface, stress oscillations associated with their deformation are not canceled by signals from adjacent volumes, and will dominate slip and stress cycling within the tabular megathrust shear zone.

At times when τ_{top} is high, we would expect deformation to temporarily shift to another volume with internal geometry more suitable for slip, which would temporarily suppress deformation within our model domain. In general, deformation within a subduction mélange would be expected to be preferentially partitioned into matrix dominated volumes; however, if clast-dominated volumes locally span the full width of the subduction thrust interface, they will be forced to deform as shear stress accumulates (Fagereng, 2011b). For example, since the CBC outcrop analogue was demonstrably deformed near peak metamorphic conditions, this volume may potentially represent part of an asperity on or just below the subduction interface.

7.2 RELATING MODEL RESULTS TO SUBDUCTION ZONE SLIP BEHAVIORS

The limitations in scale, and restriction to velocity-strengthening rheologies in our model setup, mean that it is not able to model all aspects of the seismic cycle. Nevertheless, it may still provide important insights into stress and slip cycling in a subduction zone mélange. For example, while we do not allow for the opening of tensile fractures, our models predict regions of net tensile stress within the modeled mélange, where clasts interact to create local dilation zones adjacent to zones undergoing continuous matrix frictional-viscous shearing flow, resulting in rotation of the local σ_1 direction (Fig. 3, right-hand panels). An implication of this is that the formation of tensile veins - which results from locally negative effective normal stresses (e.g., Fig. 3) – can be explained by locally elevated deviatoric stresses, rather than elevated fluid pressures. This style of deformation is consistent with the mixed continuous-discontinuous mode of deformation described in the CBC by Fagereng and Sibson (2010). The rotation of σ_1 near dilation zones can also help to explain the wide range in orientations of fractures observed in the field within the CBC (Fagereng, 2011a). This model observation of negative effective stress caused by local tension without fluid-driven hydrofracture conditions, implies that vein formation can occur without local and transient elevation in fluid pressure if local dilation arises from local deviatoric stress. Precipitation of vein quartz without hydrofracture was also suggested in dilatant sites within an exhumed accretionary prism by Lewis and Byrne (2003).

We do not include velocity-weakening effects – we instead model clasts as velocity-neutral brittle blocks in a velocity-strengthening matrix, the mineral scale deformation mechanisms of which include pressure solution and dislocation creep. However, microphysical models of quartz-phyllosilicate gouge and laboratory experiments predict a transition from velocity-strengthening to velocity-weakening behavior with increasing strain-rates, and that this transition depends on ambient pressure, temperature and matrix composition (den Hartog and Spiers, 2014; Fagereng and den Hartog, 2017). Other work has shown that the range of temperatures, pressures and strain-rates at which transitional slip behavior can occur may be enhanced in a tectonic mélange that contains clasts of brittle, competent, velocity-weakening material surrounded by a matrix of low-viscosity, incompetent, velocity-strengthening material (Biemiller and Lavier, 2017). By relating the ratio of competent to incompetent material to a smoothing factor that averages rate-state properties along a fault, they demonstrated that a heterogeneous mix of velocity-strengthening and velocity-weakening material can promote seismic slip transients. While we do not explore such processes, we show that even without prescribing velocity-weakening behavior, subduction mélanges can develop oscillations in shear stress and slip velocity

Rapid subseismic slip episodes modeled in experiment 2 may potentially be interpreted as slip transients that arise during periods of low sliding resistance to bulk shear stress. The stress and slip transients in experiments 1 and 2 occur on time periods comparable to instrumentally observed SSE events – i.e., durations of days to years (Miller et al., 2002; Rogers and Dragert, 2003; Obara et al., 2004; Peng and Gomberg, 2010), with cyclicity on timescales of months to years (Miller et al., 2002; Rogers and Dragert, 2003; Obara et al., 2004; Peng and Gomberg, 2010). While such outcrop-scale stress and slip cycling within subduction mélanges is not directly analogous to larger scale SSE or ETS on subduction interfaces (e.g., Hayman and Lavier, 2014), time periodicities are roughly comparable with those of slow slip transients observed at subduction margins (Fig. 5). For example, along the southern Hikurangi subduction margin, deep SSEs lasting ~1 – 1.5 year occur every ~5 year, while further north shallow SSEs last a few weeks and occur every 1 – 2 years (Wallace et al., 2012). Furthermore, modeled stress and strain-rate transients occur at pressure and temperature conditions for which we would also expect ETS (Ide et al., 2007). High frequency stress fluctuations in experiment 1 (with stress variations of ca. 0.1-5 MPa; Fig. 2), can lead to ephemeral pressure shadows where effective pressures approach zero, compatible with conditions under which local seismic tremor is thought to occur during slow slip in subduction zones. The observation of many small and frequent slip transient episodes in experiment 2 - with slip velocities only slightly higher than plate rates - in between much larger slip transients (slip rates >0.5 m year^{-1}; Fig. 4) is also consistent with recent studies pinpointing very small slow slip events, which suggest that a spectrum of slow slip magnitudes occur during the interseismic period (Frank, 2016). Fagereng (2011b) suggest that the frequency-size distribution of clasts within the CBC may impose a frequency-size distribution of characteristic length scales of brittle deformation in the mélange that will correspond to a range of seismic styles and earthquake magnitudes, with estimated $M_w < 0$ at the outcrop scale. However, at larger scales, these variations may be smoother; the magnitudes of our modeled, local stress changes are high compared with stress drop magnitudes inferred for non-volcanic tremor from earthquake and tidal triggering (Rubinstein et al., 2007; Houston, 2015).

8 CONCLUSIONS

We use outcrop-scale numerical models to simulate stress and strain transients within a clast-dominated tectonic mélange. Experiments where a constant boundary velocity is imposed produce shear stress cyclicity of ~ 25-80%; experiments where a constant top shear stress is imposed show transient slip episodes where slip velocities increase by 1-2 orders of magnitude. Slip transients are accomplished by mixed brittle-viscous deformation, with strain concentrated into the weaker incompetent matrix and at boundaries between adjacent competent clasts. The periodicity of stress cycling and/or slip velocity cycling, and the magnitude of slip velocity transients are comparable with observations of slow slip observed at convergent margins, while development of locally low effective stresses due to dynamic stress variations between clasts in a mélange may help to explain the occurrence of episodic tremor. Because we do not require fluctuations in fluid pressure or velocity-weakening behaviors to generate stress and strain transients, it is possible that they occur primarily as a natural consequence of progressive geometric reorganization within subduction mélanges.

9 ACKNOWLEDGMENTS

This work was funded by a Marsden Grant (GNS1204) to S. Ellis and A. Fagereng. In addition, S. Webber was partly funded by a Victoria University of Wellington Summer Research Scholarship. We acknowledge useful discussions with Carolyn Boulton, Demian Saffer, Laura Wallace, and James Biemiller. We thank Matt Ikari and an anonymous reviewer for their constructive and thought-provoking reviews.

10 REFERENCES

Araki, E., Saffer, D.M., Kopf, A.J., Wallace, L.M., Kimura, T., Machida, Y., Ide, S., Davis, E., Expedition, I., 2017. Recurring and triggered slow-slip events near the trench at the Nankai Trough subduction megathrust. Science 356, 1157-1160.

Bachmann, R., Glodny, J., Oncken, O., Seifert, W., 2009. Abandonment of the South Penninic–Austroalpine palaeosubduction zone, Central Alps, and shift from subduction erosion to accretion: constraints from Rb/Sr geochronology. Journal of the Geological Society 166, 217-231.

Bartlow, N., Wallace, L., Beavan, R., Bannister, S., Segall, P., 2014. Time-dependent modeling of slow slip events and associated seismicity and tremor at the Hikurangi subduction zone, New Zealand. Journal of Geophysical Research: Solid Earth 119, 734-753.

Biemiller, J., Lavier, L., 2017. Earthquake supercycles as part of a spectrum of normal fault slip styles. Journal of Geophysical Research: Solid Earth.

Buiter, S., Ellis, S., 2012. Benchmarking a new ALE Finite-Element code. Geophysical Research Abstracts 14.

Bukovská, Z., Jeřábek, P., Morales, L.F., 2016. Major softening at brittle-ductile transition due to interplay between chemical and deformation processes: An insight from evolution of shear bands in the South Armorican Shear Zone. Journal of Geophysical Research: Solid Earth 121, 1158-1182.

Cyprych, D., Piazolo, S., Wilson, C.J., Luzin, V., Prior, D.J., 2016. Rheology, microstructure and crystallographic preferred orientation of matrix containing a dispersed second phase: Insight from experimentally deformed ice. Earth and Planetary Science Letters 449, 272-281.

den Hartog, S., Peach, C., de Winter, D., Spiers, C., Shimamoto, T., 2012. Frictional properties of megathrust fault gouges at low sliding velocities: New data on effects of normal stress and temperature. Journal of Structural Geology 38, 156-171.

Den Hartog, S., Spiers, C., 2013. Influence of subduction zone conditions and gouge composition on frictional slip stability of megathrust faults. Tectonophysics 600, 75-90.

den Hartog, S., Spiers, C., 2014. A microphysical model for fault gouge friction applied to subduction megathrusts. Journal of Geophysical Research: Solid Earth 119, 1510-1529.

Deubelbeiss, Y., Kaus, B.J., Connolly, J.A., Caricchi, L., 2011. Potential causes for the non-Newtonian rheology of crystal-bearing magmas. Geochemistry, Geophysics, Geosystems 12.

Fagereng, Å., 2011a. Geology of the seismogenic subduction thrust interface. Geological Society, London, Special Publications 359, 55-76.

Fagereng, Å., 2011b. Frequency-size distribution of competent lenses in a block-in-matrix mélange: Imposed length scales of brittle deformation? Journal of Geophysical Research: Solid Earth (1978–2012) 116.

Fagereng, Å., Cooper, A.F., 2010. Petrology of metabasalts from the Chrystalls Beach accretionary mélange-implications for tectonic setting and terrane origin. New Zealand Journal of Geology and Geophysics 53, 57-70.

Fagereng, Å., den Hartog, S.A., 2017. Subduction megathrust creep governed by pressure solution and frictional-viscous flow. Nature Geoscience 10, 51-57.

Fagereng, Å., Remitti, F., Sibson, R.H., 2010. Shear veins observed within anisotropic fabric at high angles to the maximum compressive stress. Nature Geoscience 3, 482-485.

Fagereng, Å., Sibson, R., 2010. Melange rheology and seismic style. Geology 38, 751-754.

Fisher, D.M., Brantley, S.L., Everett, M., Dzvonik, J., 1995. Cyclic fluid flow through a regionally extensive fracture network within the Kodiak accretionary prism. Journal of Geophysical Research: Solid Earth 100, 12881-12894.

Frank, W.B., 2016. Slow slip hidden in the noise: The intermittence of tectonic release. Geophysical Research Letters 43.

Hayman, N., Lavier, L., 2014. The geologic record of deep episodic tremor and slip. Geology 42, 195-198.

Houston, H., 2015. Low friction and fault weakening revealed by rising sensitivity of tremor to tidal stress. Nature Geoscience 8, 409-415.

Hyndman, R., Wang, K., 1993. Thermal constraints on the zone of major thrust earthquake failure: The Cascadia subduction zone. Journal of Geophysical Research: Solid Earth 98, 2039-2060.

Ide, S., Beroza, G., Shelly, D., Uchide, T., 2007. A scaling law for slow earthquakes. Nature 447, 76-79.

Ikari, M., Niemeijer, A., Spiers, C., Kopf, A., Saffer, D., 2013. Experimental evidence linking slip instability with seafloor lithology and topography at the Costa Rica convergent margin. Geology 41, 891-894.

Ikari, M., Saffer, D., 2011. Comparison of frictional strength and velocity dependence between fault zones in the Nankai accretionary complex. Geochemistry, Geophysics, Geosystems 12.

Ikari, M.J., Kameda, J., Saffer, D.M., Kopf, A.J., 2015. Strength characteristics of Japan Trench borehole samples in the high-slip region of the 2011 Tohoku-Oki earthquake. Earth and Planetary Science Letters 412, 35-41.

Ji, S., Zhao, P., Xia, B., 2003. Flow laws of multiphase materials and rocks from end-member flow laws. Tectonophysics 370, 129-145.

Lewis, J.C., Byrne, T.B., 2003. History of metamorphic fluids along outcrop-scale faults in a Paleogene accretionary prism, SW Japan: Implications for prism-scale hydrology. Geochemistry, Geophysics, Geosystems 4.

Liu, Y., Rice, J.R., 2005. Aseismic slip transients emerge spontaneously in three-dimensional rate and state modeling of subduction earthquake sequences. Journal of Geophysical Research: Solid Earth (1978–2012) 110.

Liu, Y., Rice, J.R., 2007. Spontaneous and triggered aseismic deformation transients in a subduction fault model. Journal of Geophysical Research: Solid Earth (1978–2012) 112.

Mair, K., Hazzard, J.F., 2007. Nature of stress accommodation in sheared granular material: Insights from 3D numerical modeling. Earth and Planetary Science Letters 259, 469-485.

Mares, V.M., Kronenberg, A., 1993. Experimental deformation of muscovite. Journal of Structural Geology 15, 1061-1075.

Miller, M.M., Melbourne, T., Johnson, D.J., Sumner, W.Q., 2002. Periodic slow earthquakes from the Cascadia subduction zone. Science 295, 2423-2423.

Miyazaki, S., Segall, P., McGuire, J., Kato, T., Hatanaka, Y., 2006. Spatial and temporal evolution of stress and slip rate during the 2000 Tokai slow earthquake. Journal of Geophysical Research: Solid Earth (1978–2012) 111.

Niemeijer, A., Spiers, C., 2005. Influence of phyllosilicates on fault strength in the brittle-ductile transition: Insights from rock analogue experiments. Geological Society, London, Special Publications 245, 303-327.

Obara, K., Hirose, H., Yamamizu, F., Kasahara, K., 2004. Episodic slow slip events accompanied by non-volcanic tremors in southwest Japan subduction zone. Geophysical Research Letters 31.

Peng, Z., Gomberg, J., 2010. An integrated perspective of the continuum between earthquakes and slow-slip phenomena. Nature Geoscience 3, 599-607.

Reber, J.E., Lavier, L.L., Hayman, N.W., 2015. Experimental demonstration of a semi-brittle origin for crustal strain transients. Nature Geoscience 8, 712-715.

Rogers, G., Dragert, H., 2003. Episodic tremor and slip on the Cascadia subduction zone: The chatter of silent slip. Science 300, 1942-1943.

Rowe, C.D., Moore, J.C., Remitti, F., 2013. The thickness of subduction plate boundary faults from the seafloor into the seismogenic zone. Geology 41, 991-994.

Rubinstein, J.L., Vidale, J.E., Gomberg, J., Bodin, P., Creager, K.C., Malone, S.D., 2007. Non-volcanic tremor driven by large transient shear stresses. Nature 448, 579-582.

Saffer, D.M., Wallace, L.M., 2015. The frictional, hydrologic, metamorphic and thermal habitat of shallow slow earthquakes. Nature Geoscience.

Saito, T., Ujiie, K., Tsutsumi, A., Kameda, J., Shibazaki, B., 2013. Geological and frictional aspects of very-low-frequency earthquakes in an accretionary prism. Geophysical Research Letters 40, 703-708.

Scholz, C., 1998. Earthquakes and friction laws. Nature 391, 37-42.

Scholz, C., 2002. The mechanics of earthquakes and faulting. Cambridge University Press, Cambridge.

Schwartz, S., Rokosky, J., 2007. Slow slip events and seismic tremor at circum-Pacific subduction zones. Reviews of Geophysics 45.
Skarbek, R., Rempel, A., Schmidt, D., 2012. Geologic heterogeneity can produce aseismic slip transients. Geophysical Research Letters 39.
Wallace, L., Beavan, J., 2010. Diverse slow slip behavior at the Hikurangi subduction margin, New Zealand. Journal of Geophysical Research: Solid Earth (1978–2012) 115.
Wallace, L., Beavan, J., Bannister, S., Williams, C., 2012. Simultaneous long-term and short-term slow slip events at the Hikurangi subduction margin, New Zealand: Implications for processes that control slow slip event occurrence, duration, and migration. Journal of Geophysical Research: Solid Earth (1978–2012) 117.
Wang, K., Bilek, S.L., 2014. Invited review paper: Fault creep caused by subduction of rough seafloor relief. Tectonophysics 610, 1-24.

11 FIGURE CAPTIONS

Fig. 1 – Model initial set up and boundary conditions. Model set up (bottom) is based on a clast-dominated outcrop from the Chrystalls Beach Complex from Fagereng and Sibson (2010) (top). Model dimensions are repeated 45 cm to either side to avoid boundary effects, and we impose a thin 1 cm-thick clast layer at the top. Periodic material flow and free velocity boundary conditions were applied at the left and right boundaries. Material leaving the right-hand boundary is reinjected at the left-hand boundary. Black represents mudstone matrix and grey regions are competent sandstone clasts. Two types of experiments were run: in experiment 1 we applied a constant shear slip velocity at the upper boundary (V_{top}); in experiment 2 we applied a constant shear stress at the upper boundary (τ_{top}; see text for details). See Supplement S1 for more details regarding the numerical model and rheology.

Fig. 2 – Summary of results from experiment 1, showing fluctuations in shear stress at the upper boundary (τ_{top}) necessary to shear the box at a prescribed slip rate at the upper boundary (V_{top}). a) Model deformed at plate tectonic slip velocities (5 cm year^{-1}). Stress magnitudes vary cyclically by ~25-40% over timescales of months to decades, superimposed on shorter-timescale fluctuations (weeks). The 3 curves are for different fluid pressure ratios λ. b) Model deformed at slow slip velocities (3 cm week^{-1}). Stress magnitudes cycle by ~25-80% over weeks, superimposed on shorter-timescale fluctuations (days). Note that the a) and b) are run to approximately the same amount of total slip on the top of the model (3 m). Dotted lines and labels in brackets refer to times shown in Fig. 3.

Fig. 3 – Temporal snapshots showing reorganization of clasts with increasing time, corresponding to indicated locations on Fig. 2a with λ = 0.8 and V_{top} = 5 cm year^{-1}. Panels at left show clasts in black; high-strain-rate pathways (strain-rate invariant >5×10^{-9} s^{-1}) in light brown; and stress bridges (based on a threshold in shear stress τ_{xy}, where orange scale increases gradually from black (≤ 80 MPa) to orange (≥ 120 MPa) with midpoint at 100 MPa). Right-hand panels show clasts in grey, and corresponding deformation mechanisms in matrix (dislocation creep- bright orange; frictional pressure-solution creep: dark blue). The green regions have effective (dynamic) mean stress ≤ 0, even though we prescribe a constant fluid pressure/overburden ratio of 0.8 (see discussion in text). Yellow lines indicate direction of principal compressive stress, and illustrate how this direction can vary by over 45° owing to local stress perturbations. a) At 10 years the stress bridges are well developed, τ_{top} is high, and matrix shear is distributed over multiple pathways. b) At 30 years, where stress bridges are mostly absent, τ_{top} is low, and the matrix is highly interconnected with one main high strain-rate pathway. Some regions of low effective stress still occur in the matrix (right-hand panel). c) At 55 years, the clasts have inhibited matrix connectivity; high strain-rate channels have split into multiple strands and numerous stress bridges are present. Note that at the times shown, matrix deformation is concentrated into the center of the model domain where horizontal matrix interconnectivity is greatest.

Fig. 4 – Summary of results of experiment 2 for pore fluid pressure ratio λ = 0.8 and an applied top shear stress at the upper boundary τ_{top} = 32 MPa. **a)** The slip rate at the upper boundary (V_{top}) is plotted as a function of time. As stress bridges disintegrate and redevelop within the model domain, the resistance of the modeled mélange to the imposed shear stress changes rapidly. Decongestion of clasts leads to short period of rapid slip (up to m year^{-1}, lasting for ~2 days), followed by long periods where the clast congestion inhibits deformation. Bursts of rapid slip are quasi-periodic. Inset panels show the clasts (black regions), strain-rates in the matrix ($\log_{10}$ of the second strain-rate invariant), and stress bridges (regions with shear stress >100 MPa shaded in orange) for two time snapshots corresponding to a time of high slip-rates (time= 5.35 years, slip velocity = 0.18 m/year) and low slip-rates (time = 6.35 years, slip velocity = 0.025 m/year).

b) The same experiment, with V_{top} plotted as a function of slip. Background color shading indicates the non-linear relationship between time and slip, with total model slip of 0.1 m occurring in the first 0.75 years, and a further 0.1 m of slip occurring after another 3.95 and 8.5 years, respectively.

Fig. 5 – The variation in slip velocity V_{top} over a ten-year period as the shear stress applied at the top of the model shear box increases. Results are for experiment 2, with fluid pressure ratio λ = 0.8. Black, green, blue and red show increasing applied shear stress at top of box τ_{top} of 28, 30, 32 and 34 MPa. Background shaded strips indicate times where top slip velocity is greater than 5 cm/year.

Fig. 6 – Plot of the increase in slip velocity with increasing τ_{top}. Fluid pressure ratio λ = 0.8. Main panel shows slip velocity versus total slip for four different applied top shear stress values ranging from 28-34 MPa. Inset shows how maximum slip velocity (during first 0.15m of slip) increases with applied shear stress τ_{top}.

Graphical Abstract (for review)

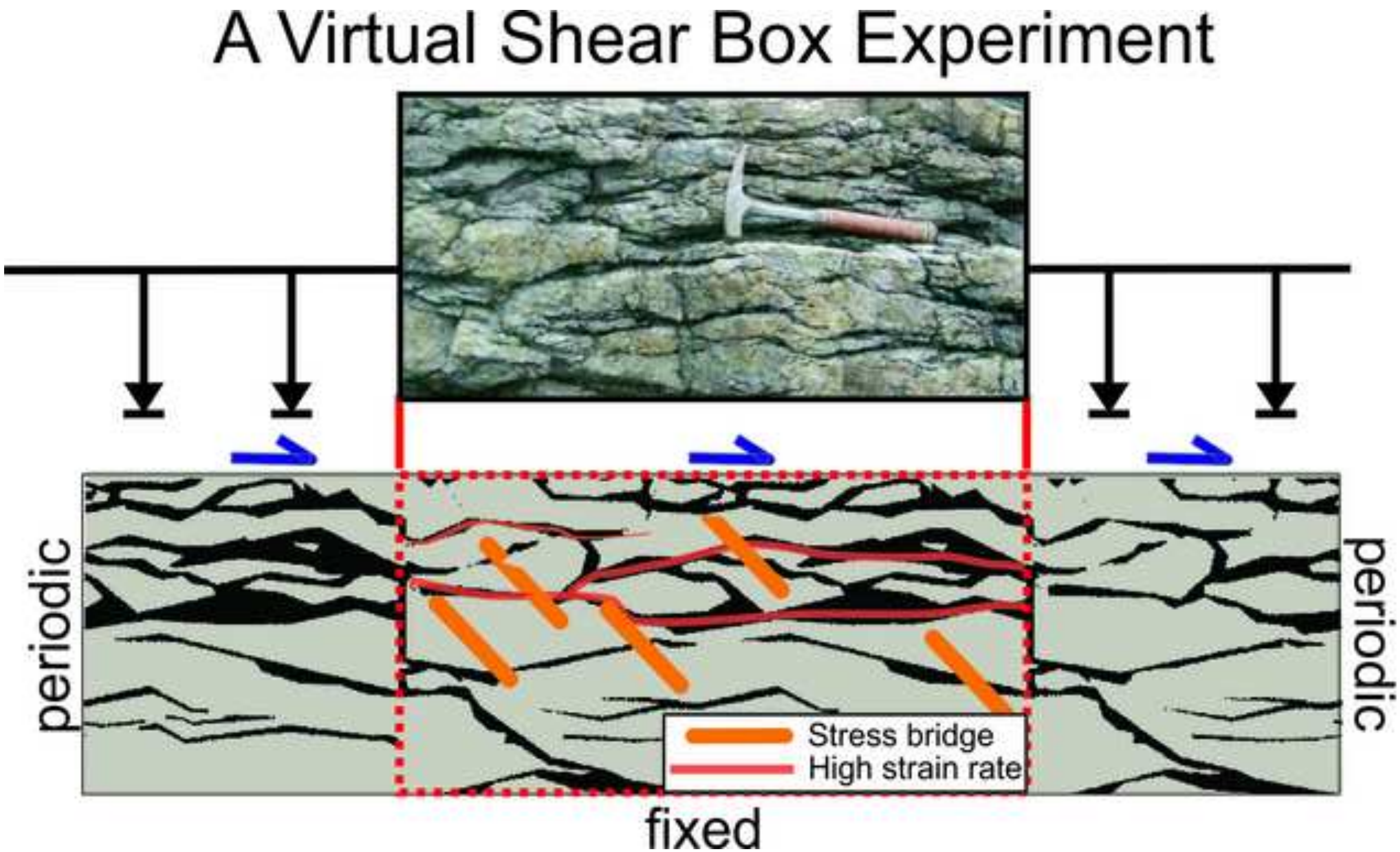

All figures

Click here to download Figure: EPSL-D-17-01036 Figures All.pdf

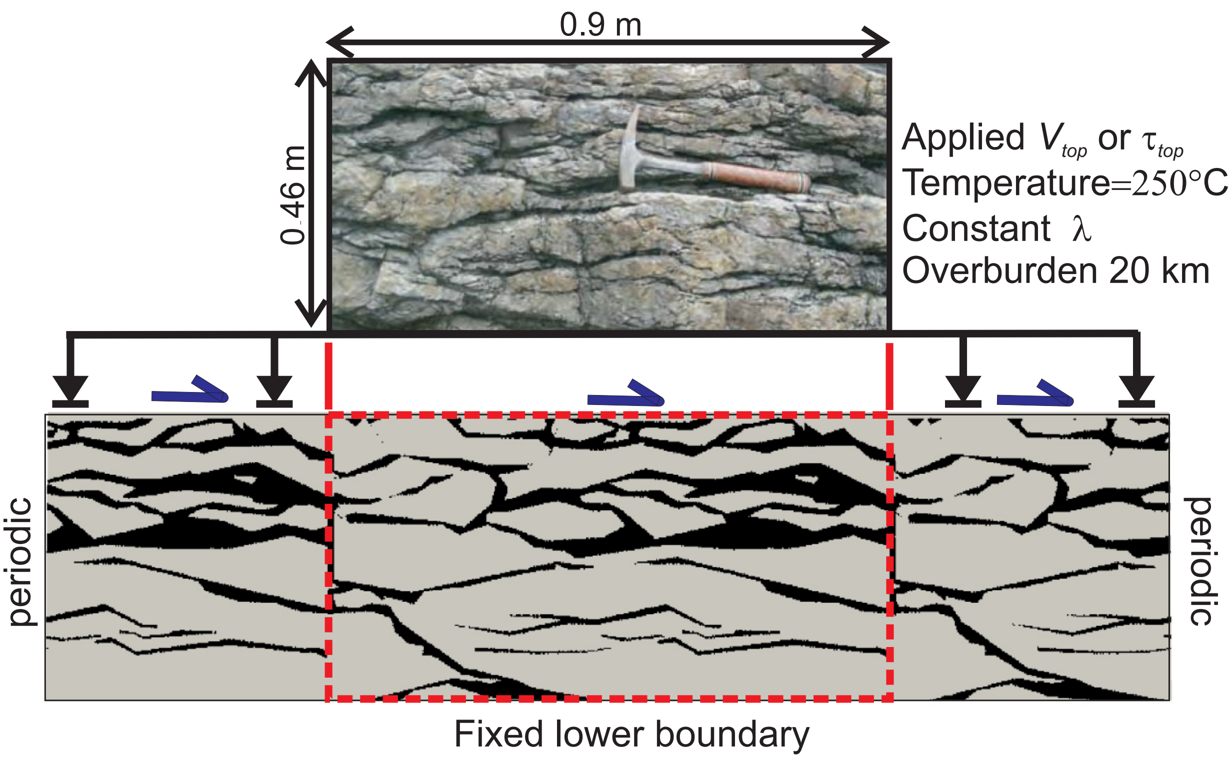

Fig. 1

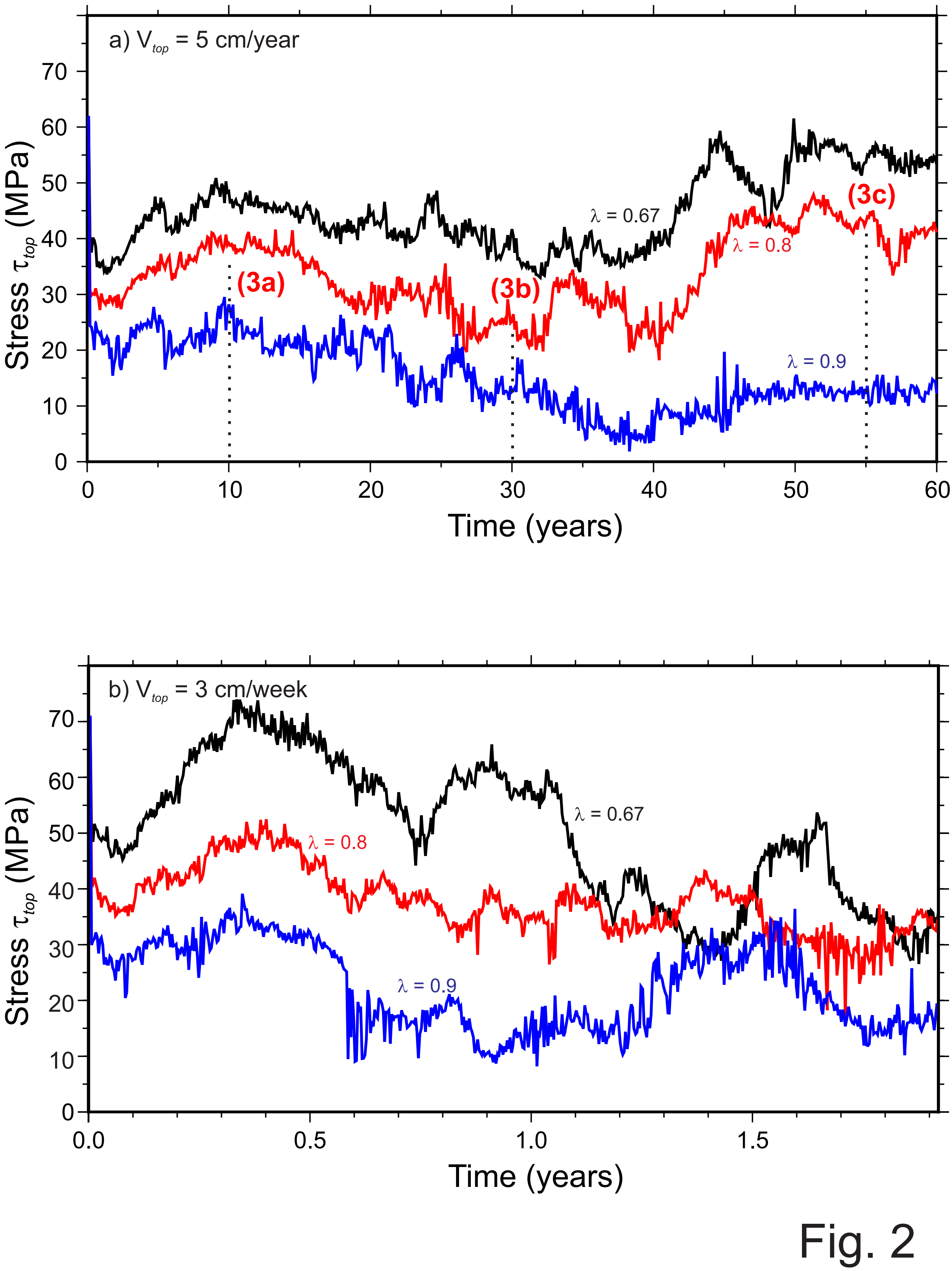

a) V_{top} = 5 cm/year
Stress τ_{top} (MPa)
Time (years)
λ = 0.67
λ = 0.8
λ = 0.9
(3a)
(3b)
(3c)
b) V_{top} = 3 cm/week
Stress τ_{top} (MPa)
Time (years)
λ = 0.67
λ = 0.8
λ = 0.9

Fig. 2

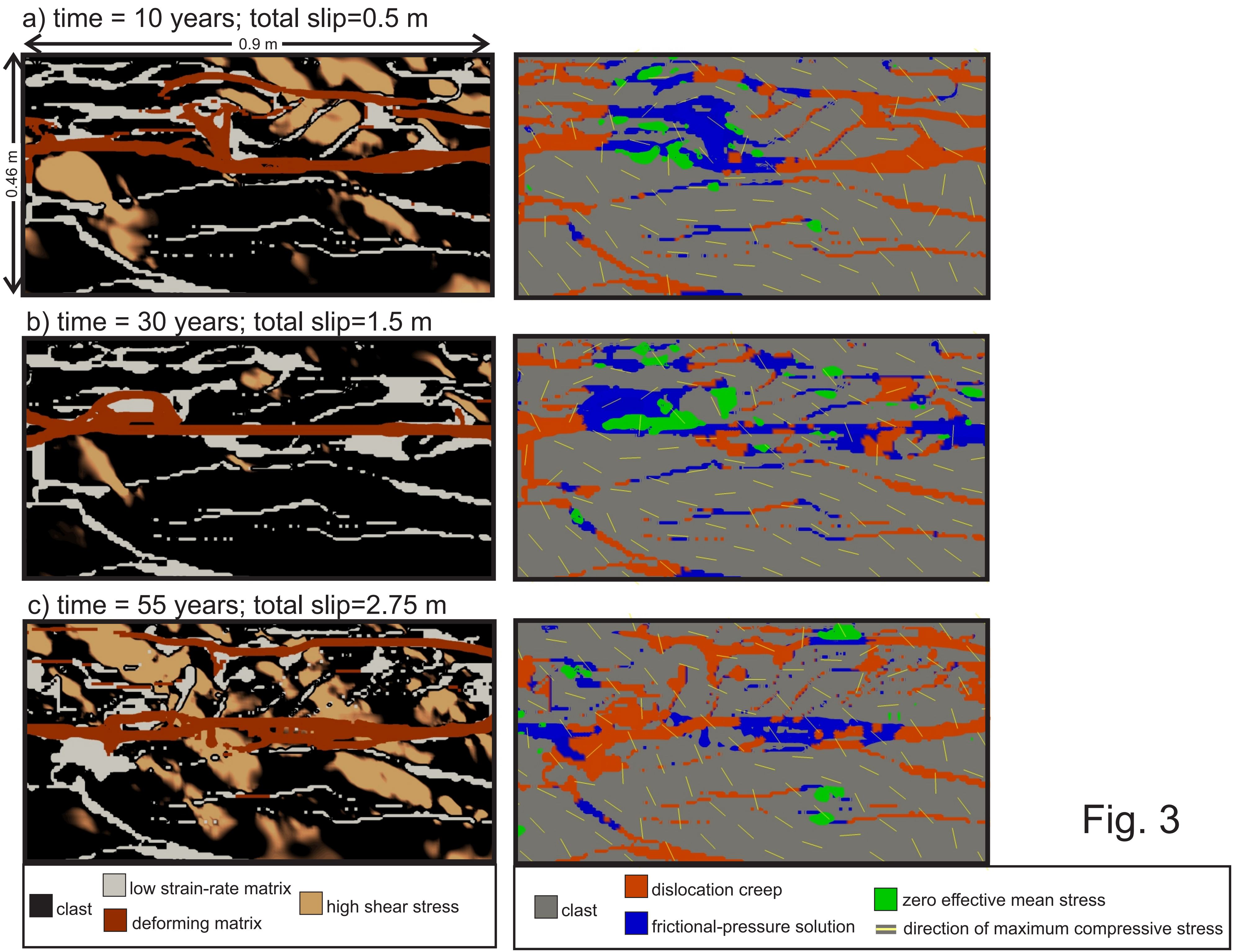
a) time = 10 years; total slip=0.5 m
0.9 m
0.46 m
b) time = 30 years; total slip=1.5 m
c) time = 55 years; total slip=2.75 m
clast
low strain-rate matrix
deforming matrix
high shear stress
clast
dislocation creep
frictional-pressure solution
zero effective mean stress
direction of maximum compressive stress

Fig. 3

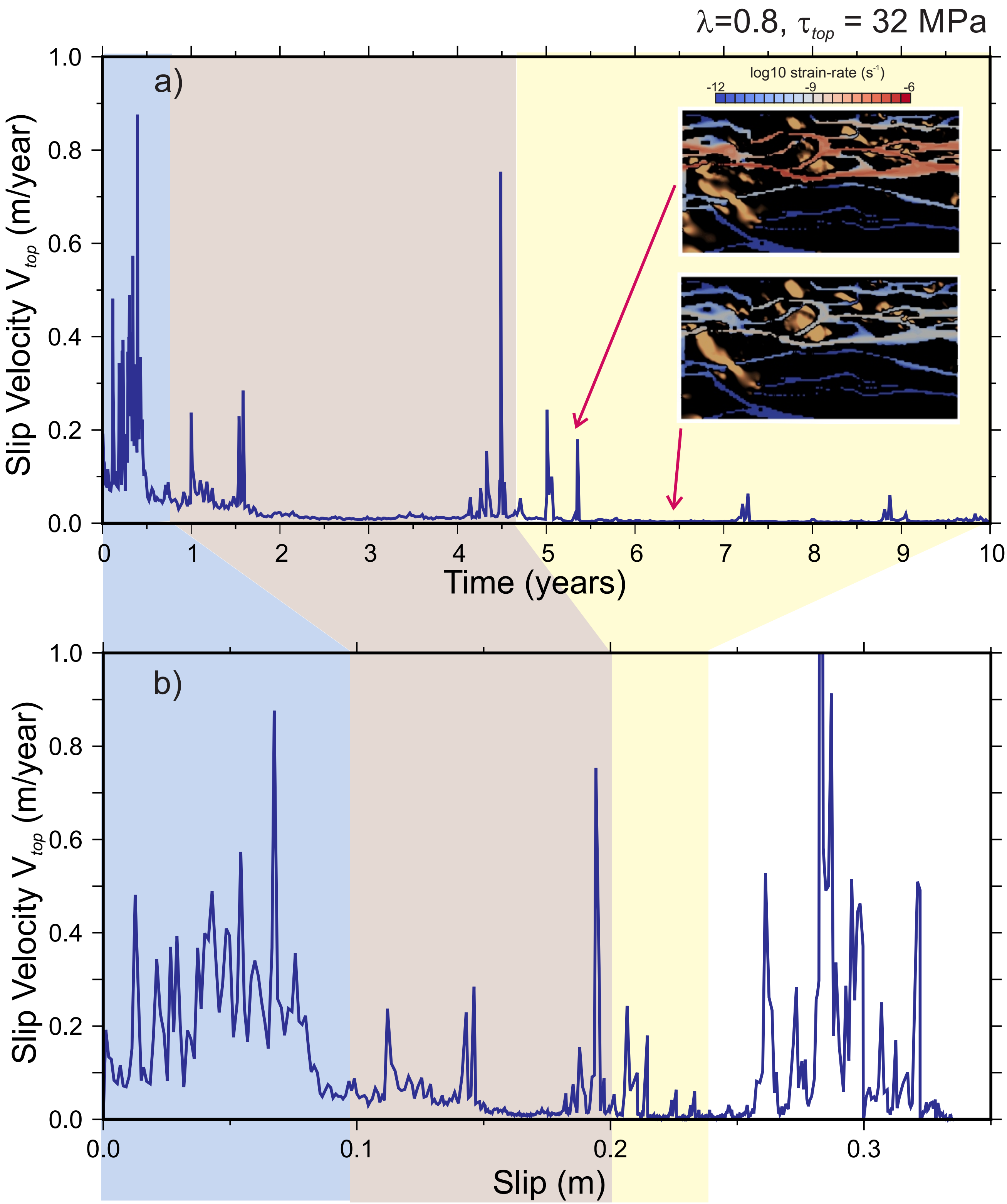
λ=0.8, τtop = 32 MPa
a)
b)
log10 strain-rate (s-1)
-12
-9
-6
Slip Velocity Vtop (m/year)
Time (years)
Slip (m)
1.0
0.8
0.6
0.4
0.2
0.0
0
1
2
3
4
5
6
7
8
9
10
0.0
0.1
0.2
0.3

Fig. 4

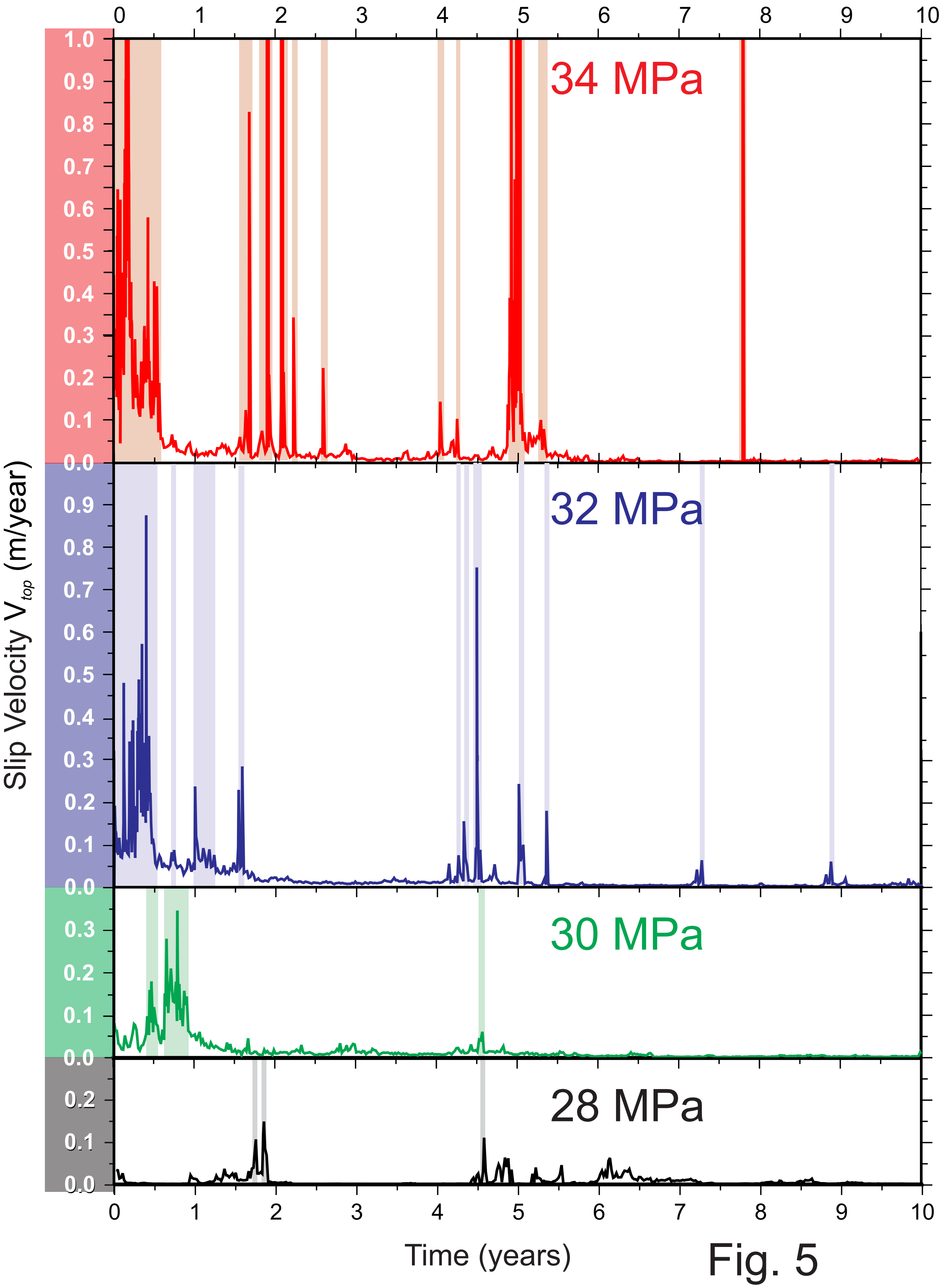
34 MPa
32 MPa
30 MPa
28 MPa
Slip Velocity V_{top} (m/year)
Time (years)
0
1
2
3
4
5
6
7
8
9
10
0.0
0.1
0.2
0.3
0.4
0.5
0.6
0.7
0.8
0.9
1.0

Fig. 5

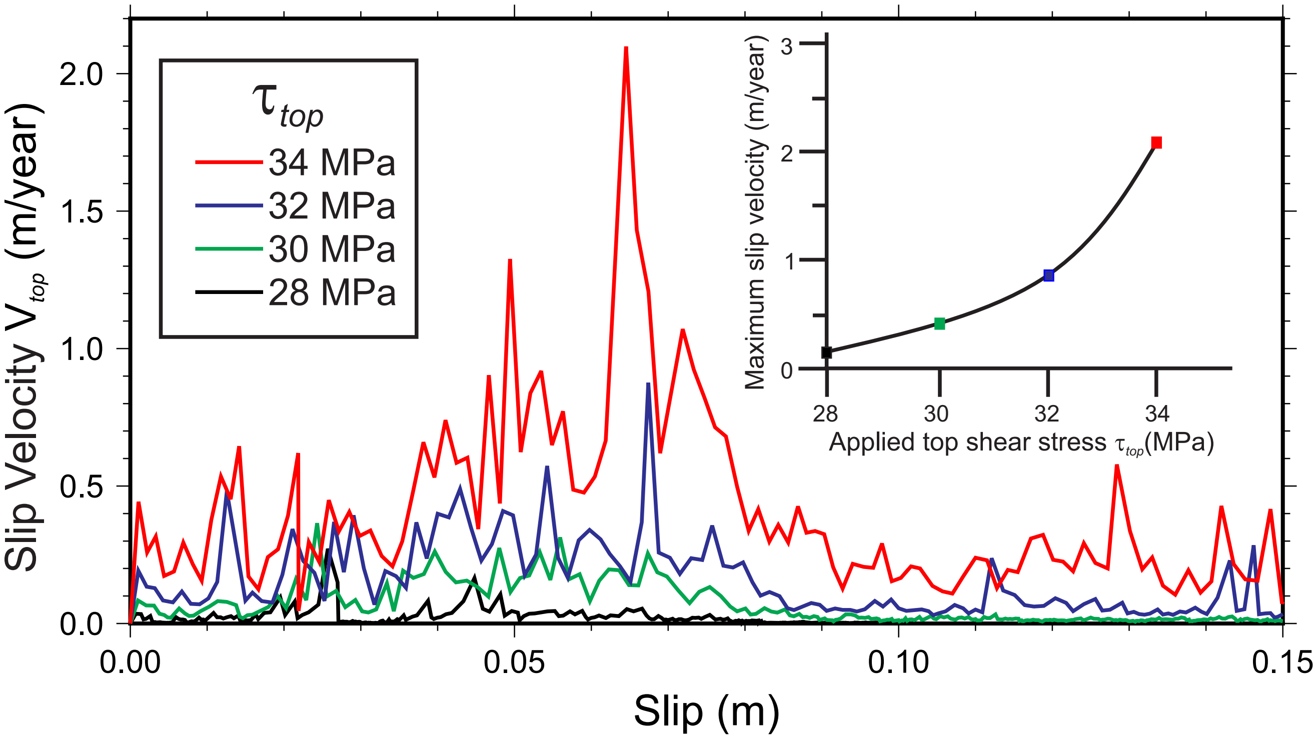

Slip Velocity V_{top} (m/year)
Slip (m)
τ_{top}
34 MPa
32 MPa
30 MPa
28 MPa
0.0
0.5
1.0
1.5
2.0
0.00
0.05
0.10
0.15
Maximum slip velocity (m/year)
Applied top shear stress τ_{top}(MPa)
0
1
2
3
28
30
32
34

Fig. 6